Intracellular Ca^{2+} Release as Irreversible Markov Process

Juliana Rengifo,* Rafael Rosales,† Adom González,* Heping Cheng,‡ Michael D. Stern,‡ and Eduardo Ríos*
*Department of Molecular Biophysics and Physiology, Rush University, Chicago, Illinois 60612 USA; †Departamento de Matemáticas, IVIC, 21827, Caracas 1020-A, Venezuela; and ‡Laboratory of Cardiovascular Science, Gerontology Research Center, NIA, NIH, Baltimore, Maryland 21224 USA

ABSTRACT In striated muscles, intracellular Ca^{2+} release is tightly controlled by the membrane voltage sensor. Ca^{2+} ions are necessary mediators of this control in cardiac but not in skeletal muscle, where their role is ill-understood. An intrinsic gating oscillation of Ca^{2+} release—not involving the voltage sensor—is demonstrated in frog skeletal muscle fibers under voltage clamp. A Markov model of the Ca^{2+} release units is shown to reproduce the oscillations, and it is demonstrated that for Markov processes to have oscillatory transients, its transition rates must violate thermodynamic reversibility. Such irreversibility results in permanent cycling of the units through a ring of states, which requires a source of free energy. Inhibition of the oscillation by 20 to 40 mM EGTA or partial depletion of Ca^{2+} in the sarcoplasmic reticulum (SR) identifies the SR $[Ca^{2+}]$ gradient as the energy source, and indicates a location of the critical Ca^{2+}-sensing site at distances greater than 35 nm from the open channel. These results, which are consistent with a recent demonstration of irreversibility in gating of cardiac Ca^{2+} sparks, (Wang, S.-Q., L.-S. Song, L. Xu, G. Meissner, E. G. Lakatta, E. Ríos, M. D. Stern, and H. Cheng. 2002. *Biophys. J.* 83:242–251) exemplify a cell-wide oscillation caused by coupling between ion permeation and channel gating.

INTRODUCTION

Rapid contraction and relaxation of vertebrate muscles require a very fast rise and fall of myoplasmic $[Ca^{2+}]$ (Rome et al., 1996). A rapid return of $[Ca^{2+}]$ to its low resting levels also minimizes deleterious consequences of increased $[Ca^{2+}]_i$, which include activation of proteolysis and signaling for apoptosis (e.g., Yu et al., 2001). It requires fast turn-off of Ca^{2+} release from the sarcoplasmic reticulum (SR), assured by two mechanisms: tight control of release channels by the membrane voltage sensor (Lacampagne et al., 2000) and an intrinsic inactivation process, independent of the voltage sensor.

The mechanisms by which Ca^{2+} release channels are activated, and then deactivated or inactivated to close, remain incompletely understood. Although the essential role of the T-tubular voltage sensor is clear, that of Ca^{2+} itself is debated. On one hand, studies of the ryanodine receptor (RyR) in subcellular preparations and lipid bilayers reveal its sensitivity to activation by Ca^{2+}, at physiologically suitable concentrations (Ca^{2+}-induced Ca^{2+} release, or CICR; Endo et al., 1970; Meissner, 1994). Hence the consensus that Ca^{2+} could mediate activation, as it does for cardiac muscle. On the other hand, tests of the mechanism in skeletal muscle fibers, usually involving the introduction of Ca^{2+} buffers, have not given clear-cut answers (Jacquemond et al., 1991; Pape et al., 1995, 1998).

The possibility that Ca^{2+} ions mediate channel inactivation is similarly debated. In whole-cell preparations, kinetic aspects of Ca^{2+} release (Schneider and Simon, 1988) and the effects of extrinsic buffers (Baylor and Hollingworth, 1988; Pape et al., 1993, 1995) or SR depletion (Pape et al., 1995, 1998), are consistent with a role of Ca^{2+}. However, physiological inactivation is extremely fast and effective. One measure (Sham et al., 1998) is the termination of Ca^{2+} release in Ca^{2+} sparks, which takes place with a half-time of 5 ms. By contrast, the concentrations of Ca^{2+} that inhibit RyRs reconstituted in bilayers are unphysiologically high, and the rates too slow. Therefore, the existence of Ca^{2+}-independent inactivation mechanisms may also be entertained (Pizarro et al., 1997).

Here we describe oscillations of Ca^{2+} release flux, which occur while the voltage sensor is steady. The oscillations are accounted for as journeys of a Markovian Ca^{2+} release unit through a set of gating states. The system oscillates because the journeys are cyclic, irreversibly driven by the SR $[Ca^{2+}]$ gradient.

The conclusion that RyRs gate irreversibly in situ was recently reached by examining the distribution of durations of Ca^{2+} release in cardiac sparks (Wang et al., 2002). The present study, in contrast, is based on global or cell-averaged aspects of Ca^{2+} release in skeletal muscle. That the conclusions are similar stresses the commonality of control mechanisms in skeletal and cardiac muscle. Evidence that the oscillation is due to coupling between channel gating and permeation supports a modulatory role of Ca^{2+} in the functional, working cell.

Submitted February 21, 2002; and accepted for publication July 12, 2002.

Address reprint requests to Eduardo Ríos, Dept. of Molecular Biophysics and Physiology, Rush University, 1750 W. Harrison St., Suite 1279 JS, Chicago, IL 60612. Tel.: 312-942-2081; Fax: 312-942-8711; E-mail: erios@rush.edu.

0006-3495/02/11/2511/11 $2.00

MATERIALS AND METHODS

Adult frogs *(Rana pipiens)* were anesthetized in 15% ethanol and killed by pithing. For cell-averaged recording of Ca^{2+} signals, singly dissected segments of fibers from the semitendinosus muscle were mounted (at 2.5–3 μm/sarcomere) in a two-Vaseline gap chamber on a modified upright microscope, under PC-based pulse generation and data acquisition (meth-

ods described in detail by González and Ríos, 1993). Experiments were carried out at 15°C. The line scan image of Fig. 1, acquired at 0.135 μm and 2 ms/pixel, was obtained at 17°C in a similarly prepared fiber by confocal microscopy of fluo-3 fluorescence (methods described in detail by González et al., 2000). For both types of experiments, the external solution filling the middle pool contained (in mM) 10 $Ca(CH_3SO_3)_2$, 130 TEA-CH_3SO_3, 5 tris maleate, 1 3,4-diaminopyridine, and 1 μM TTX. It was adjusted to pH 7 and 260 mosmol/kg. In the end pools, four formulations of a cesium glutamate-based internal solution were used, with different total [EGTA] and compensatory changes in cesium glutamate. It contained, in mM, 5 ATP, 5.5 magnesium, 10 HEPES, 5 glucose, 5 phosphocreatine, 0.8 Antipyrylazo III (or 100 μM fluo-3 in the confocal experiment illustrated). Total [EGTA] was 0.1, 5, 20, or 40 mM. $CaCl_2$ was added at a concentration equal to 0.18 [EGTA] for a nominal free $[Ca^{2+}]$ of 100 nM. The solution was adjusted to pH 7 and 270 mosmol/kg. In some experiments with 5, 20, or 40 mM EGTA, the solution also contained 1 mM Phenol Red (for simultaneous determinations of pH, a study currently in progress).

Ca^{2+} transients, release flux, and SR calcium content

Ca^{2+} transients, the averaged increases in myoplasmic $[Ca^{2+}]$ upon voltage clamp stimulation, were derived from changes in absorbance of the dye Antipyrylazo III (ApIII) as described by Shirokova et al. (1996). The concentration of dye was monitored by the resting absorbance of the cell at 550 nm, and the changes in $[Ca^{2+}]$ by changes in absorbance at 720 nm. When Phenol Red was present, dye concentrations were determined from measurements of resting absorbance at 480 and 620 nm. Because Phenol Red does not absorb light at 720 nm, the Ca^{2+}-dependent signal of ApIII is not affected by its presence. No differences were found between results obtained with or without Phenol Red in the internal solution, and the results were pooled regardless of its presence.

Ca^{2+} release flux was derived from Ca^{2+} transients by the "removal" method (of Melzer et al., 1987, modified by González and Ríos, 1993), whereby release flux is calculated as the sum of the rate of change of free $[Ca^{2+}]$ plus the combined rate of Ca^{2+} removal due to the main binding and transport processes. Removal rate is calculated using literature values of the relevant parameters, some of which are adjusted to accomplish best agreement with the decay of cytoplasmic $[Ca^{2+}]$ after release ends. The values of parameters used in the removal computations are listed in Table 1. The adjustable parameters are identified by a range of values in the table.

The initial calcium content in the SR (Ca_{SR}) was estimated by a method of Schneider et al. (1987b), which assumes that permeability is constant during the quasi-steady phase of release. In experiments in which long duration voltage pulses of large amplitude were applied, the integral of release flux during the high-voltage pulses of long duration tended asymptotically to a maximum level. Such asymptote provided a close alternative to the "constant permeability" estimate of Ca_{SR}. The alternative is necessary as some of the present results challenge the main tenet of the method of Schneider et al. (1987b).

Intramembranous charge movement

Membrane current was recorded simultaneously with optical signals. The solutions and pulse protocols were suitable to determine intramembranous charge movements (González and Ríos, 1993) up to a voltage of ~ -35 mV. Charge movement transients, $I_Q(t)$, were derived from the asymmetric current (test minus scaled control at -120 mV) by subtraction of sloping baselines fitted to late portions of ON and OFF transients. Charge transfer was obtained by integration of I_Q over time.

TABLE 1 Values of parameters used by the release flux algorithm

Parameter	Value
Fluo-3/Ca ON-rate	3.2×10^7 M^{-1} s^{-1}
Fluo-3 dissoc. const.	1.03 μM
EGTA/Ca ON-rate	$2–4 \times 10^6$ M^{-1} s^{-1}*
EGTA/Ca OFF-rate	1.5-4 s^{-1}*
Troponin/Ca ON-rate	5.7×10^6 M^{-1} s^{-1}
Troponin/Ca OFF-rate	11.4 s^{-1}
Parvalb/Ca ON-rate	1.25×10^8 $M^{-1}s^{-1}$
Parvalb/Ca OFF-rate	0.5 s^{-1}
Parvalb/Mg ON-rate	3.3×10^4 M^{-1} s^{-1}
Parvalb/Mg OFF-rate	3 s^{-1}
ATP/Ca ON-rate	1.4×10^8 M^{-1} s^{-1}
ATP/Ca OFF-rate	3.0×10^4 s^{-1}
ATP/Mg ON-rate	1.95×10^6 M^{-1} s^{-1}
ATP/Mg OFF-rate	1.95×10^2 s^{-1}
Maximum pump rate	1–4 mM s^{-1}*
[Pump sites]	0.1 mM‡
[Troponin]	0.24 mM
[Parvalbumin]	1 mM
[EGTA]	0.1–40 mM†
[ATP]	5 mM

Resting $[Ca^{2+}]$ was 0.1 μM unless noted otherwise. $[Mg^{2+}]$ was 0.6 mM.
*Parameters were changed within range given, for best agreement of the calculated evolution and the measured time course of $[Ca^{2+}]$ after the end of the voltage pulses. See Melzer et al., 1987, for details.
†Equal to concentration in internal solution.
‡Assumed in instantaneous equilibrium with $K_D = 1$ μM.

Theoretical methods

A formula to calculate the stationary increase in $[Ca^{2+}]$ due to the presence of an open channel was derived from general expressions by Pape et al. (1995), adapted to the case when two buffers (EGTA and ATP) are present.

The steady-state increase $\Delta[Ca^{2+}](r)$ due to one open channel was calculated as y_0/r, where r is distance from the open channel and

$$y_0 = \frac{\phi}{2\pi n'_A D_{Ca}} + \sum_{i=1}^{2} c_i y_i \equiv \Phi + \sum_{i=1}^{2} c_i y_i \qquad (1)$$

where ϕ is the flux in ions s^{-1}, D_{Ca} is the Ca^{2+} diffusion coefficient, n'_A is the number of ions in one thousandth of a mole, i is 1 for EGTA and 2 for ATP, c_i is D_i/D_{Ca}, and y_i are elements of a column vector

$$\mathbf{U\,D\,e} - \Phi\mathbf{A}^{-1}\mathbf{f}. \qquad (2)$$

where $\mathbf{A}$ is a 2×2 matrix of elements $A_{ii} = a_i + b_i$ and $A_{ij} = a_i\, c_j/c_i$, with $a_i = k_i\, L_i/D_{Ca}$, k_i the forward Ca^{2+}-binding rate constant of buffer i, L_i its concentration, $b_i = (k_i\,[Ca^{2+}]_R + k_i)/D_i$, $[Ca^{2+}]_R$ is resting $[Ca^{2+}]$, and k_i^- the backward rate constant. $\mathbf{U}$ is the matrix of unit eigenvectors of $\mathbf{A}$ in column, $\mathbf{f}$ the column vector of elements a_i/c_i, and $\mathbf{e}$ the column vector of terms $\exp(-r/\sqrt{\lambda j})$, where λj are the eigenvalues of $\mathbf{A}$. Finally, $\mathbf{D}$ is a diagonal 2×2 matrix, whose diagonal terms form the column vector

$$\Phi\mathbf{JCf} \qquad (3)$$

and $\mathbf{J}$ is the Jordan form of $\mathbf{A}$. (Equations 1–3 are, with minor modifications, two-dimensional versions of equations B19, B29, and B32 of Pape et al., 1998.)

RESULTS

An oscillation of Ca^{2+} release, not determined by the voltage sensor

In a skeletal muscle fiber, the time course of Ca^{2+} release flux during an action potential or a voltage clamp pulse reflects the evolution of RyR channel open probability, plus a concomitant decay in driving force due to partial depletion of SR calcium (Schneider and Simon, 1988). Under voltage clamp, release flux usually goes through an early peak, then decays monotonically to a quasi-steady level, severalfold lower (reviewed by Ríos and Pizarro, 1991). Maylie et al. (1987) and Maylie and Hui (1991) were the first to show that Ca^{2+} transients elicited by a voltage step could be oscillatory. Shirokova et al. (1994) traced the oscillation in the Ca^{2+} transient to an oscillation in Ca^{2+} release.

As described by Shirokova et al. (1994), the oscillation is best seen in fibers near slack length (no more than 3 μm per sarcomere) at voltages a few tens of millivolts from the resting potential. Fig. 1*A* shows an oscillating response to a -45 mV pulse, in a confocal line scan of fluorescence. In this spatially resolved view, the oscillation appears as a transient dip in the frequency of Ca^{2+} sparks after the initial peak. Other aspects of the oscillation are better seen in "global" or "cell-averaged" Ca^{2+} release records (illustrated in Fig. 1 *B*).

Using intracellular electrodes, Shirokova et al. (1994) demonstrated that membrane potential was stable and spatially homogeneous during the oscillations, which were recorded in the virtual absence of ionic currents. They found that oscillations of Ca^{2+} release were accompanied by an oscillation in intramembranous charge movement current, believed to reflect gating movements of the T membrane voltage sensor. As illustrated in Fig. 1, however, the long-lasting oscillations reported here far outlast the oscillations in charge movement. Record *B* is release flux, derived from the Ca^{2+} transient elicited by a pulse to -50 mV. Trace *C* plots the charge movement current I_Q, and record *D* its running integral Q(*t*) or "charge transfer." In this example, Q(*t*) does not increase monotonically, but decays after a peak, corresponding to a small negative I_Q (the significance of which is still debated: cf. Shirokova et al., 1994, with Jong et al., 1995). In this and most records studied, Q(*t*) reached a steady value 20 to 50 ms into the pulse, while the oscillation of Ca^{2+} release continued, sometimes for hundreds of milliseconds. The oscillation that remains after Q(*t*) becomes steady must be intrinsic to the release process.

As shown in Fig. 2, the oscillation had a steep dependence on voltage. Its amplitude, measured by the fractional difference ((*S*−*W*)/*S*) between release in the first well (*W* in Fig. 1 *B*) and the steady level *S*, decreased with increasing depolarization, vanishing at -35 mV. Meanwhile, its kinetics accelerated, as if the voltage sensor somehow determined the oscillation rate. The increase in frequency with

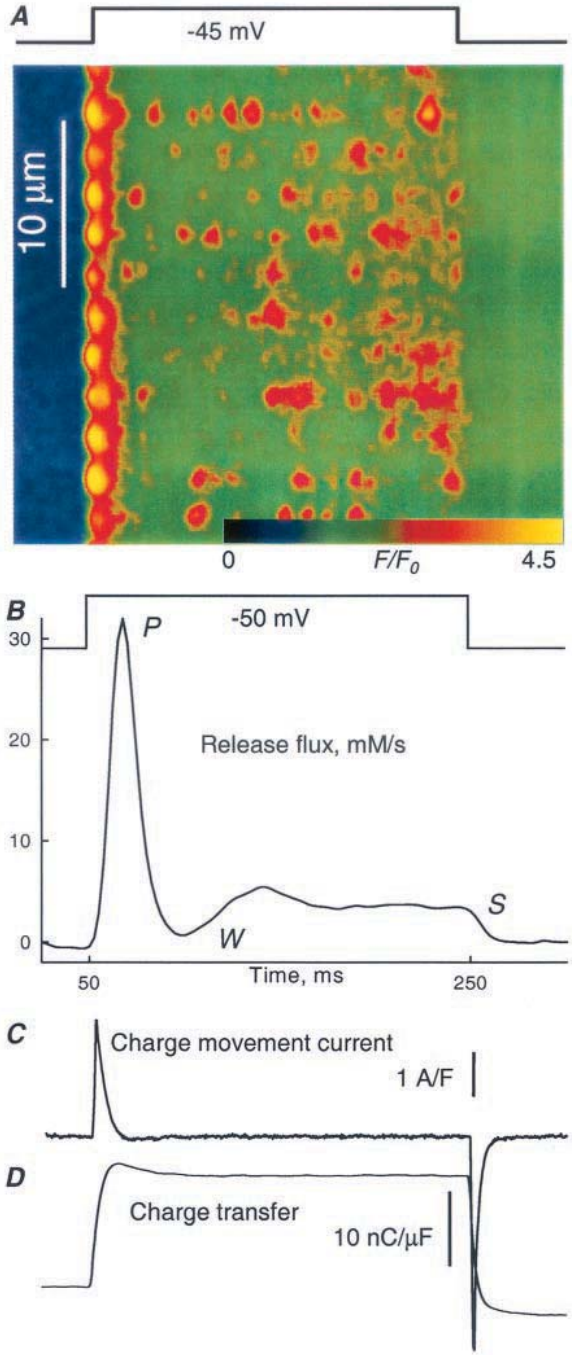

FIGURE 1 Oscillation in release flux with steady voltage sensor. (*A*) Line scan image of fluo-3 fluorescence in voltage clamped fiber, upon 200 ms depolarization to -45 mV. Fluorescence $F(x, t)$, normalized to baseline average $F_0(x)$ (see Methods and González et al., 2000). ID 0928a26. (*B*) Ca^{2+} release flux elicited by clamp pulse at top, derived from a "whole-cell" Ca^{2+} transient in a different fiber. *P*, *W*, and *S* levels are used to quantify the oscillation. (*C*) Simultaneously recorded charge movement current (normalized to fiber's linear capacitance). (*D*) "Charge transfer" Q(*t*) (integral of current). Fiber exposed 100 min to the internal solution with 5 mM EGTA. Ca^{2+} release flux was calculated by the "removal" method, with EGTA/Ca OFF rate constant = 2 s^{-1}, maximum pump rate = 4 mM s^{-1}, and other parameter values in Table 1. Linear capacitance, 10.6 nF. ID 1641E, #49.

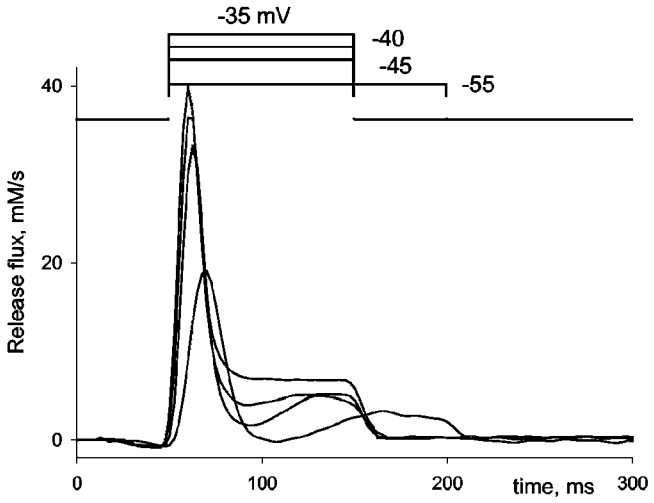

FIGURE 2 Voltage-dependent kinetics of the oscillation. Release records derived from transients elicited at different voltages, as indicated, in the presence of 5 mM EGTA in the internal solution. Note reduction in oscillation amplitude and increase in frequency with voltage. Release flux was calculated by the removal method, with the same parameter values as in Fig. 1. ID: 1641E #56–59.

voltage, and the eventual elimination of the oscillation at −35 or −30 mV, were observed in every fiber studied.

A model makes testable predictions

This observation suggested a model, detailed later, in which the channels cycle unidirectionally among three states: *closed*, *open*, and *inactivated* (see Fig. 5 *A*). If all channels in the ensemble start from *closed*, then the collective cycling will initially result in macroscopic oscillations of the ensemble. Although these will die out, cycling will continue indefinitely. Such cycling requires a source of free energy.

Many sources could conceivably provide the energy for cycling. A partial list includes the electric field across the plasmalemma and T membrane, the electric field across the SR membrane, SR pumping and other chemical reactions, including phosphorylation reactions, driven by ATP hydrolysis, and the $[Ca^{2+}]$ gradient between SR and cytoplasm. The plasmalemmal electric field was ruled out. Indeed, to draw energy from an electric field requires moving charge. One type of moving charge, ions, cannot be involved, as their passage can be entirely blocked without consequences. The other type, intramembranous charge, cannot mediate the energy input either, because oscillations of Ca^{2+} release continue long after the intramembranous charge movement has ceased. Among the other putative sources, some are especially unlikely (like a transient SR potential). Transport by the SERCA pump will fluctuate with $[Ca^{2+}]_{cyto}$ or $[Ca^{2+}]_{SR}$, but is an unlikely driver of an oscillation that is best seen at very low levels of release. While there were no a priori arguments for or against other putative sources, involvement of the SR $[Ca^{2+}]$ gradient seemed readily testable.

If this gradient, or the consequent increase in $[Ca^{2+}]_{cyto}$ upon channel opening were required for the oscillation, high Ca^{2+} buffering of the cytoplasm and reduction of the $[Ca^{2+}]$ gradient, together or separately, should reduce or eliminate the oscillation. These predictions were tested in the experiments that follow.

TABLE 2 Effect of EGTA on the oscillation

EGTA (mM)	*n*	*V* (mV)	*P* (mM/s)	*W* (mM/s)	*S* (mM/s)	(*S*−*W*)/*S*	(*P*−*S*)/*P*
0.1	5	−51.0	3.54	0.64	1.02	0.33	0.67
			0.91	0.10	0.22	0.08	0.05
5	7	−52.1	13.66	1.06	2.04	0.44*	0.84
			3.79	0.34	0.49	0.10	0.01
20	4	−46.3	6.21	1.44	1.68	0.13	0.72
			1.45	0.32	0.41	0.02	0.03
40	6	−45.0	6.02	2.00	2.14	0.06	0.60
			2.03	0.48	0.50	0.03	0.05

Averages and SEM (italics) of oscillation parameters. *n*, numbers of fibers at each [EGTA]; *V*, average test voltage; *P*, peak release flux; *W*, its value at the first minimum (illustrated in Fig. 1); *S*, the steady value, calculated as the average during the last 20 ms of a 120 ms depolarization, or the last 50 ms of a 200 ms depolarization. (*S*−*W*)/*S* quantifies the oscillation, while (*P*− *S*)/*P* quantifies the fractional inactivation by the end of the pulse.
*Value at 5 mM is different than at 20 or 40 mM at $p < 0.05$ in two-tailed *t*-tests.

The oscillation was suppressed in high EGTA

The oscillations were compared with different concentrations of EGTA in the internal solution, in the range 0.1 to 40 mM. In all experiments, the release waveform was measured after more than 100 min of equilibration with the end pool solution. Therefore, [EGTA] in the working segment was probably equal to or greater than in the solution. The flux values *P*, *W*, and *S* (defined in Fig. 1 *B*) were determined at the voltage that gave the greatest oscillation. Results are summarized in Table 2.

(*P*−*S*)/*P*, quantifying inactivation, and (*S*−*W*)/*S*, quantifying the oscillation, are plotted against [EGTA] in Fig. 3. Increasing [EGTA] had a biphasic effect on the magnitude of the oscillation, essentially abolishing it at 40 mM. In fact, only one of six fibers studied at this concentration had a sizable oscillation, and it was one with exceptionally high release and SR calcium content (identifier 1726E01). The effects of increasing [EGTA] on the magnitude of inactivation, (*P* − *S*)/*P*, were much smaller, albeit in the same direction as the effects on the oscillation.

The oscillation was suppressed by SR depletion

The second prediction of a Ca^{2+}-dependent model, that the oscillation should wane as SR Ca^{2+} is depleted, was tested most effectively in 40 [EGTA] in the one cell that showed

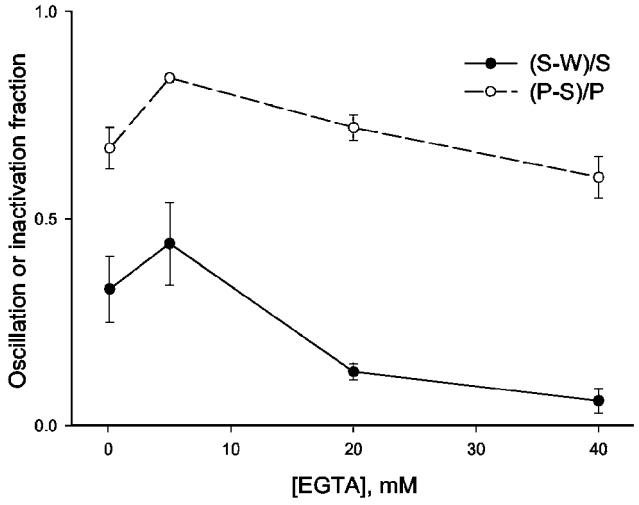

FIGURE 3 Oscillations in various concentrations of EGTA. Levels *P*, *W*, and *S*, defined in Fig. 1, were measured for every record obtained at the voltage that elicited the greatest oscillation, in different fibers exposed to four different [EGTA]. Numbers of fibers in each condition are given in Table 2. Symbols mark averages and bars span ± SEM at each concentration. [EGTA] has a major effect on the magnitude of the oscillation (*filled symbols*) and a modest effect on the susceptibility to inactivation (*open symbols*). Release flux was calculated in every case assuming [EGTA] equal to the nominal concentration in the internal solution, EGTA/Ca ON rate constant between 2×10^6 M^{-1} s^{-1} and 4×10^6 M^{-1} s^{-1}, OFF rate constant between 1.2 and 4 s^{-1}, maximum pump rate between 1 and 4 mM s^{-1} and values of other parameters given in Table 1.

a large oscillation (1726E01). At lower [EGTA] qualitatively similar results were obtained, but were often complicated by movement during depleting depolarizations. Fig. 4 illustrates a three-pulse protocol, consisting of identical reference and test pulses at −45 mV, and an intercalated depleting depolarization at +60 mV. Represented are release flux records for three realizations of the protocol, with different durations of the depleting pulse. Other realizations, at 10, 100, 400, and 1000 ms duration, are not shown.

A voltage clamp pulse, or the release that it elicits, have three types of effects on subsequent responses: inactivation of the voltage sensor, effects associated with depletion (Schneider et al., 1987b) and an inactivation operating directly on the release system. The inactivation of the voltage sensor requires depolarizations of many seconds (Brum et al., 1988). Direct release inactivation recovers nearly exponentially, with a time constant of 100 ms or less (Schneider and Simon, 1988; Pape et al., 1993). In the experiments illustrated, an interval of 1100 ms ensured recovery from inactivation. Therefore, the effects monitored were largely limited to those of depletion. As shown best in the inset, where test release records are superimposed in time, there was a reduction in release flux as depletion increased. There were also prominent kinetic effects, including elimination of the oscillation after the depletion pulses of duration 200 ms or greater.

Integrating over time the release flux records in Fig. 4, it was found that the conditioning patterns released 2.9, 6.2, or 8.7 mM Ca^{2+} by the end of the depleting pulse of 200 ms, 700 ms, or 1400 ms, respectively. The total content of Ca^{2+} in the resting SR of this fiber was estimated at 10.1 mM, an unusually high value. At the time when the test pulses were applied, the remnant was estimated to be 23%, 41%, and 73%, respectively. (These numbers were reached estimating SR Ca^{2+} replenishment in the intervening 1.1 s to be proportional to the decay in free [Ca^{2+}] measured during the interval. Without taking this restoration into account, the remnants would be 14, 38, and 72%, respectively.) While these methods to measure release flux are subject to errors of scale (discussed, for instance, by González and Ríos, 1993), they yield reliable representations of time course (Schneider et al., 1987a), especially when mM [EGTA] is present (Ríos and Pizarro, 1991; Sham et al., 1998, Pape et al., 1998). Because the estimate of SR calcium content derives from the flux of release, a similar qualification applies to Ca_{SR}. While its total may be in error, the estimates of fractional release and depletion should be more robust.

The initial SR calcium content in the experiment of Fig. 4 (1726E01) was two to three times greater than in the other experiments with 40 mM EGTA. That its reduction to 73% was sufficient to abolish the oscillation in this fiber may explain the absence of oscillation in the others. Their Ca_{SR} was already <73% of that in the exceptional experiment.

THEORY AND DISCUSSION

The time course of release induced by a constant depolarization, and its associated permeability, usually have the biphasic form of the top record of Fig. 2 (−35 mV), namely an initial peak followed by a monotonic relaxation to a sustained phase that decays much more slowly. Oscillations of release flux were first demonstrated by Shirokova et al. (1994), and interpreted as a by-product of feedback coupling between release channels and voltage sensors (another manifestation of which is the delayed "I_γ" component of intramembranous charge movement). In their view, the oscillation in Ca^{2+} release and that in charge movement were causally linked, therefore inseparable.

That view must be revised. As shown with the present results, the oscillation in release may outlast by 100 ms any visible oscillation in charge movement. The oscillation is therefore intrinsic to the release channels, and in this sense analogous to the fast inactivation that terminates the early peak of flux. In the following we derive the necessary conditions to produce oscillations in the simplest model of a release unit. Interpreted in such context, the oscillations reveal an interaction between the channels and Ca^{2+}, requiring a gradient of [Ca^{2+}] from SR lumen to cytosol.

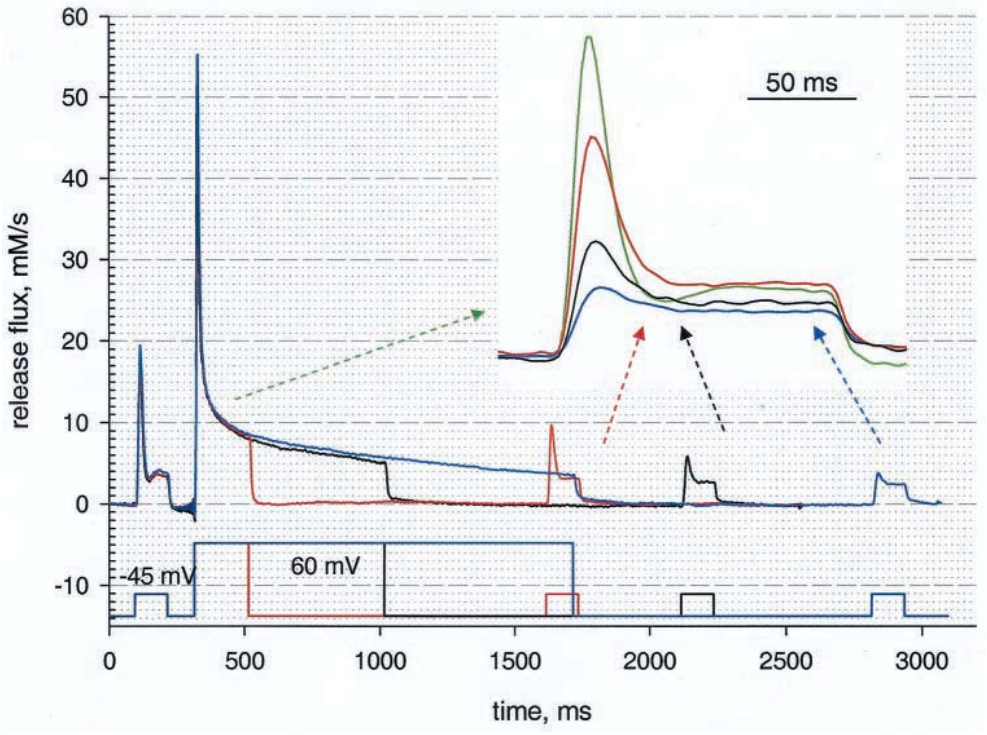

FIGURE 4 Effects of depletion on the kinetics of oscillatory release. Shown are three release flux records, among several of a sequence obtained at 5 min intervals, after ≈100 min of exposure to 40 mM EGTA. Each record exhibits release elicited by a pattern of three pulses plotted in matching color. Patterns consist of a −45 mV, 120 ms reference pulse, followed by a depleting pulse of variable duration to +60 mV, then a recovery interval of 1100 ms and a test pulse to −45 mV. Illustrated are depletion durations of 200 (*red*), 700 (*black*), and 1400 ms (*blue*). *Inset:* test portions of records and average of all references (*green*). Note the major kinetic changes in test release induced by different durations of the depleting pulse. Release records were derived from Ca^{2+} transients assuming [EGTA] = 40 mM, EGTA/Ca ON rate constant = 2.5×10^6 M^{-1} s^{-1}, EGTA/Ca OFF rate constant = 2 s^{-1}, maximum pump rate = 4 mM s^{-1}, and values of other parameters given in table 1. ID 1726E01, #22, 24, 27.

Oscillatory relaxations of a Markov chain

In the (millisecond) time scales of interest for this system, RyR channels are probably Markovian, i.e., their future depends on the present only. The alternative, channels with transition rates that depend on history, becomes unappealing upon examining the physical processes that can endow the channels with millisecond-range memory. The best candidate for such role is the change in cytoplasmic [Ca^{2+}], which spans many milliseconds. It appears, however, that the gating effects of Ca^{2+} require concentrations of several μM, which are only reached locally, near the channels' cytoplasmic opening, and are established or dissipated rapidly (e.g., Stern, 1992). In such cases, even Ca^{2+}-influenced transition rates will appear fixed to the millisecond-scale observer, and the system will effectively be Markovian and homogeneous (i.e., with transition rates not explicitly time-dependent).

In Fig. 5 *A* is one such model. It is meant as a simple phenomenological representation of a "release unit," an unspecified group of interacting channels. The evolution of p_{open}, the occupancy of the open state, is

$$p_{open}(t) = A_0 + A_1 \exp(-\lambda_1 t) + A_2 \exp(-\lambda_2 t) \quad (4)$$

where the eigenvalues λ_1, roots of the characteristic equation of the system, are a function of the transition rates (Colquhoun and Hawkes, 1995, p. 600). $p_{open}(t)$ will be oscillatory if at least one of the eigenvalues is complex (in fact two, because eigenvalues occur as conjugate pairs). In the following it will be demonstrated that for this to happen, the Markov process must be irreversible (i.e., not in equilibrium). This will be done by showing that the eigenvalues of processes gating in equilibrium are real.

Denote by (X_t), $t \geq 0$, a Markov process (in which time is continuous, e.g., Norris, 1997) that can assume any of the states i in a discrete set or state space E, associated to a particular gating mechanism. (Every transition is "reversible" in the sense that the reciprocal is allowed, but this does not guarantee microscopic reversibility, defined below). The state occupation density at time t is defined as the vector $\mathbf{p}(t) = [p_i(t)]$, with $p_i(t)$ = probability$(X_t = i)$. The evolution of this density, representing the relaxation of the process, is given by

$$\mathrm{p}(t) = \mathrm{p}(0)e^{\mathrm{Q}t}, \quad (5)$$

where $\mathbf{Q}$ is the transition rate matrix of elements q_{ij}, $i, j \in E$. The diagonal elements q_{ii} are negative or zero, while the

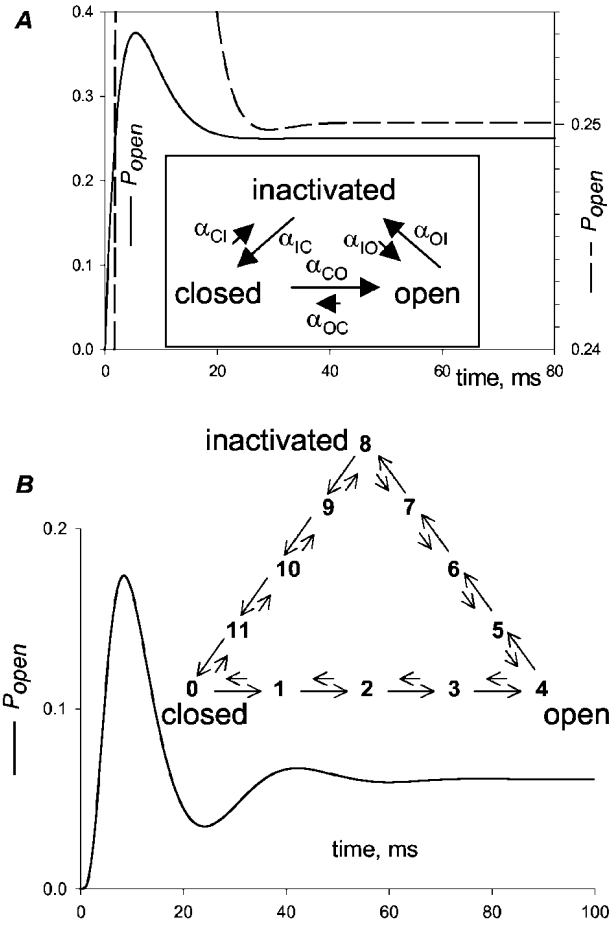

FIGURE 5 Oscillations in Markovian models. (*A*) P_{open} versus time during a relaxation of the model diagrammed in the box. Initial condition: $P_{closed} = 1$. Rate constants (in s^{-1}): $\alpha_{CO} = 200$, $\alpha_{OI} = 200$, $\alpha_{IC} = 100$; reverse constants equal to 1/1000 of the forward ones. The dashed curve is a 20× enlargement to show the oscillation. As justified in the Appendix, the oscillation amplitude could not be significantly increased by changing parameter values. (*B*) P_4 versus time during a relaxation of the model illustrated—a generalization of the model in (*A*). $\alpha_{j\to j+1} = 500\ s^{-1}$ for all j except 11. $\alpha_{11\to 0} = 100\ s^{-1}$, $\alpha_{j+1\to j} = 50\ s^{-1}$.

nondiagonal elements are positive or zero and $\Sigma_{j\in E}\, q_{ij}=0$ for all i (Norris, 1997, Section 2.1). If **Q** is assumed to have r distinct eigenvalues $\lambda_1, \ldots, \lambda_r$, then it is similar to a diagonal matrix, i.e., admits the form $\mathbf{Q} = \mathbf{UJU}^{-1}$, where **J**, or $\mathbf{d}(\lambda_1, \ldots, \lambda_r)$ is the Jordan form of **Q**, an $r \times r$ matrix with λ_1 as diagonal elements and zeros elsewhere, and **U** is the (left) matrix of change of basis (a nonsingular matrix with r unit eigenvectors as columns). In this case, Eq. 5 yields

$$\mathbf{p}(t) = \mathbf{p}(0)\ \mathbf{U}\ \mathbf{d}(e^{\lambda_1 t}, \ldots, e^{\lambda_r t})\mathbf{U}^{-1} \tag{6}$$

The process (X_t) is *time-reversible* if there exists a set of occupation numbers satisfying $\pi_i \geq 0$, $\Sigma_{i\in E}\, \pi_i = 1$, such that opposite transitions are balanced one to one (or "in detail"), that is:

$$\pi_i q_{ij} = \pi_j q_{ij}, \quad \text{for } i, j \in E. \tag{7}$$

Using Eq. 7 it can be seen that, if the process is time-reversible, then **Q** is similar to a symmetric matrix **Q***,

$$Q^* = D^{1/2} Q D^{-1/2}, \tag{8}$$

with $\mathbf{D} = \mathbf{d}(\pi_1, \ldots, \pi_r)$. Because of its symmetry, all the eigenvalues of **Q*** are real (Horn and Johnson, 1990). Because of similarity with **Q***, those of **Q** are the same. Thus, from Eq. 6 it follows that (X_t) relaxes monotonically, without oscillations.

Furthermore, it can be shown that every gating model with individually reversible steps but without cycles is time-reversible, implying that models must have cycles, or rings of states, to be irreversible. Indeed, a model without cycles can be divided by any cut between two states in two separate parts, say *A* and *B*. Because in the steady state the total probability flow out of *A*, given by $\pi_A\, q_{AB}$, must equal the total flow into *A*, $\pi_B q_{BA}$, it follows that the probability flows across the cut, i.e., between i and j, satisfy detailed balance. Hence, any mechanism with no cycles relaxes monotonically.

In sum, for a Markov process to relax with oscillations, it must have a cycle *and* breach the condition of detailed balance. This rules out the possibility that the oscillations result from transitions between two states. The three-state model of Fig. 5 *A* satisfies the requisites when the product of the rate constants α_{CO}, α_{OI}, and α_{IC} is greater than that of the three others. When the system starts with the probability concentrated in *closed*, the cycling is accompanied by macroscopic oscillations of p_{open}. As shown in Fig. 5 *A*, the oscillation is visible but very small. As shown in general in the Appendix, oscillations of three-state models are damped, and small, with a ratio between the first well and the first peak not greater than 0.043.

Fig. 5 *B* shows a generalization of the model in *A*, with three "pre-open" states in the activation pathway, and similar intermediates in each side. The p_{open} transient is now very similar to the experimental ones. Cycling and the oscillation will become faster with increasing voltage because the activation pathway is part of the cycle (and is necessarily voltage-dependent).

Despite this success, the model robustly fails to reproduce the sharp decay of oscillation amplitude with voltage. The details of the release waveform probably will not be reproduced without adding a more detailed picture of interactions between channels. One parsimonious addition is the assumption that Ca^{2+} mediates the interactions. This will be shown later to naturally explain the effect of voltage.

In conclusion, Markovian chains with constant transition rates can exhibit the oscillating behavior, provided that they cycle irreversibly. The effects of EGTA and the depletion protocols are consistent with the idea that the energy source for this cycling is the Ca^{2+} concentration difference between SR and cytosol.

The oscillations are coupled to the [Ca^{2+}] gradient

For the oscillation to be coupled to the concentration gradient it is not enough that gating be Ca^{2+}-sensitive. The sensitivity must break detailed balance (Eq. 7) only when there is a Ca^{2+} gradient between SR and cytoplasm. The inhibitory effects of EGTA indicate that the elevated [Ca^{2+}] must act on the cytoplasmic side of the channels upon their own opening or the opening of neighbors. One possibility is that cytoplasmic Ca^{2+} binding increases the opening rate constant α_{CO} substantially (Fig. 5 *A*). If no other transition rate changes, then detailed balance is breached. This is of course a CICR scenario. A second possibility is the increase in the rate constant α_{OI}, which again leads to irreversible cycling and possible oscillations. This is Ca^{2+}-dependent inactivation. Thus, CICR and Ca^{2+}-dependent inactivation constitute the two simplest explanations of the oscillation. Both have the same thermodynamic consequence, to push the system off equilibrium, causing it to cycle permanently (and oscillate transiently).

Thermodynamic feasibility

The energy source in the concentration gradient should be sufficient to account in excess for the decrease in free energy around the irreversible cycle. Such loss was compared with the chemical potential in the SR [Ca^{2+}] gradient. Take as an example the 12-state ring of Fig. 5, which gives a realistic oscillation. Multiplying all equilibrium constants $K_{j\,j+1}$ around the ring (the value of which is 10 except for $K_{11\,0}$, with a value of 2), the result, 2×10^{11}, corresponds to a $\Delta G = 26.02\ RT$. Assuming [Ca^{2+}] = 1 mM inside the SR and 100 nM in the cytosol, the chemical potential difference is 9.21 *RT*. These numbers imply that a minimum of three Ca^{2+} ions should deliver their energy to drive the cycling.

Gating coupled to the permeant ion

When channels are modulated by the permeant ions, irreversible gating (coupled to downhill ion movement) becomes possible. Actual observations of the predicted consequences of such coupling are rare. At the level of single channels they include non-monotonic histograms of open times and asymmetric (i.e., time-irreversible) currents (Lauger, 1985). Asymmetric currents were reported for a Torpedo Cl^- channel (Richard and Miller, 1990) and traced to the collaborative role of Cl^- and voltage in its gating (Chen and Miller, 1996). Asymmetric transitions between substates were also found for a mutant NMDA channel (Schneggenburger and Ascher, 1997) and a modal distribution of open times was reported for glutamate channels of the locust (Gration et al., 1982). The present results constitute the first case where irreversible gating results in a global, cell-wide observable, the oscillation. The scarcity of examples is surprising, considering that many plasmalemmal channels interact with their permeant species. The theory of Markov processes developed above, showing that steady irreversibility requires a ring of states, suggests an explanation. Oscillations may be fundamentally impossible in plasmalemmal channels, due to the lack of a cycle, a return pathway from *inactivated* to *closed* that does not simply retrace the forward steps.

At the level of single channels the signal consequence of nonequilibrium is the appearance of non-monotonic dwell time distributions (Colquhoun and Hawkes, 1995). Open times of Ca^{2+} release units map to rise times of Ca^{2+} sparks. That these have modal distributions (as shown by González et al., 2000, for mammalian muscle, and Wang et al., 2002 (and less directly Bridge et al., 1999) for cardiac cells), indicates nonequilibrium gating of the unit. By contrast, the open time distributions of reconstituted RyRs are monotonic, even when Ca^{2+} is the permeant ion. Therefore, the irreversibility results from interactions lost in the reconstituted system (Wang et al., 2002). The interactions could be among channels or with additional molecules. The analysis that follows suggests interactions among multiple channels.

Properties of the Ca^{2+}-sensing site

The two interventions applied here do not equivalently alter the free Ca^{2+} concentration. While depletion scales the concentrations evenly, the presence of buffers has relatively greater effects at greater distances from the channel pore. As shown by Pape et al. (1995), this circumstance may be used to constrain the location and affinity of the site(s) involved.

We calculated the concentration of cytoplasmic Ca^{2+} in the vicinity of an open channel, under four different conditions simulating the experiments. EGTA and ATP were included in the calculation, at the concentrations present in the internal solutions. Because the calculated profiles were in steady state, no fixed buffers were taken into account. We used analytic solutions to the linearized problem, developed by Pape et al. (1995, 1998; cf. generalization by Smith et al., 2001), which parse the increase as $\Delta[Ca^{2+}]_p + \Delta[Ca^{2+}]_o$. $\Delta[Ca^{2+}]_p$ is due to an open channel, with unitary flux ϕ, located at $r = 0$. $\Delta[Ca^{2+}]_o$ is the joint contribution by the ensemble of other channels. This joint effect was calculated by addition of individual channel contributions. The steady contribution of one open channel is given in Methods (Eqs. 1–3). Such a linear approach seems justified by evidence that the indicator dye is not saturated near open channels (an absence of flat top sparks, a reported lack of correlation between amplitude and spatial half-width of experimentally measured sparks, and their similar spatial properties in simulations with varying source current). Lack of saturation of the dye suggests that other, lower-affinity reactions of Ca^{2+} proceed in a near-linear range.

It is assumed that channels in the ensemble (contributors to $\Delta[Ca^{2+}]_o$) form an array of two rows in register, with 30

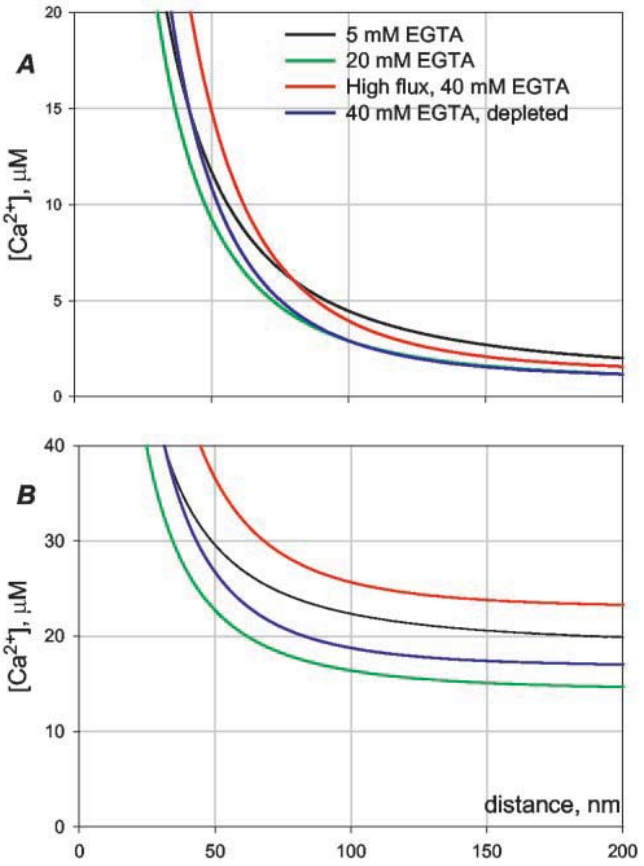

FIGURE 6 Steady-state $[Ca^{2+}]$ near open channels. $[Ca^{2+}]$ is plotted versus distance from an open channel. As described in Methods and Pape et al. (1995), the increment $\Delta[Ca^{2+}]$ is calculated as the sum of $\Delta[Ca^{2+}]_p$, contribution by the channel at $r = 0$, with unitary fluxϕ, plus $\Delta[Ca^{2+}]_o$, contribution by a double row of channels located at 30 nm intervals with flux 0.0058 ϕ (*A*) or 0.063 ϕ (*B*). Black and green traces represent standard fibers ($\phi = 2.25 \times 10^6$ ions per second) with total [EGTA] = 5 mM or 20 mM. Red and blue traces represent the exceptional fiber 1726E01, with 40 mM [EGTA], and $\phi = 4.5 \times 10^6$ ions per second in the reference condition (*red*), or 3.285×10^6 ions per second in the condition reached after a 200 ms depleting pulse. Diffusion coefficients (in units of 10^{-6} cm^2 s^{-1}): Ca, 3: EGTA or EGTA Ca, 1.7; ATP or ATP Ca, 1.4. ON rate constants (10^6 M^{-1} s^{-1}): EGTA/Ca, 2.5; ATP/Ca, 136. OFF rate constant (s^{-1}): Ca/EGTA, 2; Ca/ATP (3×10^4). Total [ATP], 5 mM.

nm between neighbors. For these, flux per channel was ϕ scaled down by the average p_{open}. One estimate of p_{open}, 0.0058, was obtained as the ratio of release flux at the time of the oscillation (i.e. 3.5 mM s^{-1} in Fig. 1) and its theoretical maximum, found by multiplying ϕ and the concentration of release channels (0.27 μM; Pape et al., 1995). An alternative estimate of p_{open} during the oscillation, 0.063, was obtained for the experiment in Fig. 4 assuming $p_{open} = 1$ at the peak of the depleting pulse. The curves in Fig. 6, *A* and *B* were calculated, respectively, with the low and the high estimate of p_{open}.

In both panels, the curves in black were calculated with 5 mM total EGTA, assuming a flux $\phi = 2.25 \times 10^6$ ions s^{-1} (or 0.75 pA, as in bilayer measurements by Kettlun et al., 2000, of Ca^{2+} currents through frog channels in near-physiological gradients). Because this was an ideal condition for the observation of oscillations, the curve defines a region of {$[Ca^{2+}]$, r} space where the dissociation constant (K_D) and distance from the channel opening (r_s) are most probably located. The red curve corresponds to the exceptional fiber 1726E01, which gave oscillations in the presence of 40 mM EGTA. Because the flux and SR calcium content of this fiber were approximately double the average in the other experiments, $[Ca^{2+}](r)$ was calculated with $\phi = 4.5 \times 10^6$ ions s^{-1}. The intersection of the curves in black and red gives a better estimate of r_s and K_D. The curve in green was calculated with the standard value of ϕ and 20 mM total EGTA. Because experimentally this condition reduced the oscillation substantially, green line and axes delimit an excluded region of {$[Ca^{2+}]$, r} space. Finally, the blue line represents the exceptional experiment after the 200-ms depletion pulse, with unitary flux reduced to 73% of its reference value. It delimits another excluded region. This leaves 75 nm and 6 μM as preferred estimates of r_s and K_D, and the crossing of the curves in black and blue at $r \approx 40$ nm as a lower limit of r_s. In panel *B*, where the higher estimate of $\Delta[Ca^{2+}]_o$ was used, the curves representing the two favorable conditions (black and red) do not cross, but come close at ≈120 nm and 13 μM. The intersection of the curves in black and blue, lower limit of r_s, remains robustly near 35 nm.

In summary, the analysis constrains the critical site to be at least 35 nm away from the open channel, and its dissociation constant at between 6 and 13 μM. While the approximations are crude and the results depend on the values of buffer parameters, the conclusion reflects the fact that EGTA may abolish the oscillation, which requires a site relatively distant from the source. It also explains its steep suppression with increasing voltage. As pointed out by Pape et al. (1995) the contribution to local $[Ca^{2+}]$ by the *ensemble* of channels ($\Delta[Ca^{2+}]_o$) is greater than that by a specific open channel ($\Delta[Ca^{2+}]_p$), except within nanometers of the open channel. A good example is in Fig. 6 *B*, where increasing p_{open} from 0.0058 to 0.063 resulted in an upward shift of $[Ca^{2+}](r)$ by ≈ 10 μM, nearly doubling the level at $r = 50$ nm. These effects of open channels help explain naturally the rapid saturation of the oscillation at higher voltages. Ca^{2+} sites that determine the oscillation should have an oscillating occupancy. Moderate increases in p_{open}, expected upon increasing depolarization, will saturate this occupancy.

Distances of 35 to 100 nm span several channels in the array. Multi-channel groups have been identified as sources of Ca^{2+} sparks (González et al., 2000). Coupling between channels, mediated by Ca^{2+} and hence fed by its concentration gradient, is a possible source of irreversibility. The couplon simulations of Stern et al. (1997, 1999), which implement such coupling, naturally yield modal distributions of open times, and may produce oscillating averages.

It is therefore not necessary to invoke mechanisms other than CICR and/or Ca^{2+}-dependent inactivation to explain the oscillations at the molecular level.

To explain the effects of EGTA, fura-2, and partial depletion, Pape et al. (1995, 1998) invoked the participation of an inactivation site, located 22 nm away from the pore. Their estimate does not necessarily contradict the present one, which is based on an oscillation absent in their observations. Perhaps a larger release current, spread over a greater group of channels, is a requisite for the oscillation. The group of interacting channels, each having one or more modulatory Ca^{2+} sites, may look to these coarse monitoring tools as one source, with a "site" whose location depends on the intensity and extent of the interaction.

Comparison with other [Ca^{2+}] oscillations and its models

Calcium oscillations, often involving IP_3-sensitive channels, have been found in many animal cells (Goldbeter, 1996). The present observation, a nonpropagated oscillation that attenuates over a few cycles, contrasts with what in most other cases are sustained oscillations, which may include spatial propagation (waves).

As formally demonstrated by Schuster et al. (2002) a minimum of two variables, one of which must be $[Ca^{2+}]_{cyto}$, are necessary for a system of kinetic equations to oscillate. The minimal models of calcium oscillations usually consider store calcium (Ca_{ER}) as the second variable, while the concentration of [IP_3] is considered a constant that needs to be at a high level to enable the oscillation, a role formally similar to that of membrane voltage in the present example.

Simple models without plasmalemmal fluxes are effectively one-variable (as $Ca_{cyto} + Ca_{ER} =$ constant). Then, to oscillate, the model must have a third calcium compartment, or perhaps a different variable (for example, p_{open}). Therefore, Schuster et al. (2002) arrive by a very different path at a conclusion isomorphic with a key property derived in the present work, that a system must have a ring of states to oscillate.

In most of the existing models the oscillation involves, explicitly or implicitly, the SR/ER content and the ER pump. It is in this regard that the model presented here may be most distinctive; it does not contemplate a role for depletion or the pump, and $[Ca^{2+}]_{cyto}$ only plays an enabling role, because the cycling continues in the absence of oscillations in $[Ca^{2+}]_{cyto}$, after the macroscopic oscillations die out.

While the present model's greatest appeal is to be a simple paradigm of nonequilibrium cycling, its crucial aspects can be supported by experiment. For example, the preferential observation of oscillations at low activation levels is inconsistent with an essential oscillation of SR content, or SERCA pumping.

In the present model, the oscillation is intrinsic to the individual release unit (or spark generator). Evidence of nonequilibrium gating of the spark generator includes, in addition to the modal distribution of open and closed times (Wang et al., 2002; González et al., 2000) a recent demonstration that multiple sparks arising at the same triad in conditions of low activation are due to repeated activation of the same unit (Butler and Klein, 2002). An ensemble of intrinsically cycling units accounts well for key aspects of the global oscillation. Because sparks are by definition local, the oscillation will not propagate. The global oscillation, a consequence of synchronization of the local oscillators, will eventually vanish, due to inevitable loss of synchronization in repeated cycles.

Irreversibility is a local property

The main conclusion of the present paper is that the oscillation manifests at the cell-averaged level the intrinsically nonequilibrium gating of the spark generators. Because the irreversibility is already present at the spark level, no additional interactions are required in principle to explain the global behavior. One may conclude that all interactions are local, implying that they take place within a few hundred nanometers. The conclusion enhances the relevance of Ca^{2+} sparks as elementary events that have sufficient complexity to account for most features of cellular function.

APPENDIX

In this appendix an exact expression is found for the maximum amplitude of the possible oscillations of a three-state homogeneous Markov process, represented in Fig. 5 *A*.

Define $S = \sum_{j=1}^{6} k_j$ and

$$T = \alpha_{OC}\alpha_{CI} + \alpha_{IO}\alpha_{IC} + \alpha_{OI}\alpha_{CO} + \alpha_{OC}\alpha_{IO} + \alpha_{OC}\alpha_{OI} + \alpha_{CO}\alpha_{IC} + \alpha_{CI}\alpha_{IO} + \alpha_{CO}\alpha_{CI} + \alpha_{OI}\alpha_{IC}$$

The non-zero eigenvalues of the system are

$$\tfrac{1}{2}(-S + \sqrt{S^2 - 4T}) \quad \text{and} \quad \tfrac{1}{2}(-S - \sqrt{S^2 - 4T})$$

Oscillatory solutions are of the form $e^{-at}\sin(bt + c) + d$ with $a = \tfrac{1}{2}S$; $b = \tfrac{1}{2}\sqrt{4T - S^2}$

The oscillation is obviously damped ($a > 0$). The first positive peak occurs (approximately) at $t = \pi/2b$, while the first negative peak occurs at $t = 3\pi/2b$. Hence the ratio of their amplitudes is $e^{-\pi a/b}$. Because $4T \le 2S^2$, then $b \le a$ and the ratio of amplitudes is less than $e^{-\pi} = 0.043$.

This work was supported by grants from the National Institutes of Health (to E.R.) and intramural research programs of National Institutes of Health (to M.D.S. and H.C.).

REFERENCES

Baylor, S. M., and S. Hollingworth. 1988. Fura-2 calcium transients in frog skeletal muscle fiber. *J. Physiol.* 403:151–192.

Baylor, S. M., and S. Hollingworth. 1998. Model of sarcomeric Ca^{2+} movements, including ATP Ca^{2+} binding and diffusion, during activation of frog skeletal muscle. *J. Gen. Physiol.* 112:297–316.

Bridge, J. H., P. R. Ershler, and M. B. Cannell. 1999. Properties of Ca^{2+} sparks evoked by action potentials in mouse ventricular myocytes. *J. Physiol.* 518(Pt.2):469–478.

Brum, G., R. Fitts, G. Pizarro, and E. Ríos. 1988. Voltage sensors of the frog skeletal muscle membrane require calcium to function in excitation-contraction coupling. *J. Physiol.* 398:475–505.

Butler, T., and M. G. Klein. 2002. Are multiple Ca^{2+} sparks in a triad activated independently? *Biophys. J.* 82:1367.

Chen, T., and C. Miller. 1996. Nonequilibrium gating and voltage dependence of the C1C-0 C1 channel. *J. Gen. Physiol.* 108:237–250.

Colquhoun, D., and A. G. Hawkes. 1995. The principles of the stochastic interpretation of ion-channel mechanisms. *In* Single Channel Recording, 2nd Ed., Chapt. 18, B. Sakmann and E. Neher, editors. Plenum Press, New York. 397–482.

Endo, M., M. Tanaka, and Y. Ogawa. 1970. Calcium induced release of calcium from the sarcoplasmic reticulum of skinned skeletal muscle fibers. *Nature.* 228:34–36.

Goldbeter, A. 1996. Biochemical Oscillations and Cellular Rhythms. Cambridge University Press, Cambridge.

González, A., W. G. Kirsch, N. Shirokova, G. Pizarro, G. Brum, I. N. Pessah, M. D. Stern, H. Cheng, and E. Ríos. 2000. Involvement of multiple intracellular release channels in calcium sparks of skeletal muscle. *Proc. Natl. Acad. Sci. U.S.A.* 97:4380–4385.

González, A., and E, Ríos. 1993. Perchlorate enhances transmission in skeletal muscle excitation-contraction coupling. *J. Gen. Physiol.* 102:373–421.

Gration, K., J. Lambert, R. Ramsey, R. Rand, and P. Usherwood. 1982. Closure of membrane channels gated by glutamate receptors may be a two-step process. *Nature.* 295:599–601.

Horn, R. A., and C. R. Johnson. 1990. Matrix Analysis. Cambridge University Press, Cambridge. Jacquemond, V., L. Csernoch, M. G. Klein, and M. F. Schneider. 1991. Voltage-gated and calcium-gated calcium release during depolarization of skeletal muscle fibers. *Biophys. J.* 60:867–873.

Jong, D. S., P. C. Pape, and W. K. Chandler. 1995. Effect of sarcoplasmic reticulum calcium depletion on intramembranous charge movement in frog cut muscle fibers. *J. Gen. Physiol.* 106:659–704.

Kettlun, C., A. González, W. Nonner, E. Ríos, and M. Fill. 2000. Ryanodine receptor (RyR) unitary Ca^{2+} current is greater in frog skeletal muscle than in mammalian heart. *Biophys. J.* 78:2576.

Lacampagne, A., M. G. Klein, C. W. Ward, and M. F. Schneider. 2000. Two mechanisms for termination of individual Ca^{2+} sparks in skeletal muscle. *Proc. Natl. Acad. Sci. U.S.A.* 97:7823–7828.

Lauger, P. 1985. Ionic channels with conformational substates. *Biophys. J.* 47:581–590.

Maylie, J., and C. S. Hui. 1991. Action of 2,3-butanedione monoxime on calcium signals in frog twitch fibers containing antipyrylazo III. *J. Physiol.* 442:551–567.

Maylie, J., M. Irving, N. L. Sizto, and W. K. Chandler. 1987. Calcium signals recorded from cut frog twitch fibers containing antipyrylazo III. *J. Gen. Physiol.* 89:83–143.

Meissner, G. 1994. Ryanodine receptor/Ca^{2+} release channels and their regulation by endogenous effectors. *Annu. Rev. Physiol.* 56:485–508.

Melzer, W., E. Ríos, and M. F. Schneider. 1987. A general procedure for determining the rate of calcium release from the sarcoplasmic reticulum in skeletal muscle fibers. *Biophys. J.* 51:849–863.

Norris, J. R. 1997. Markov Chains. Cambridge University Press, Cambridge.

Pape, P. C., D. S. Jong, and W. K. Chandler. 1995. Calcium release and its voltage dependence in frog cut muscle fibers equilibrated with 20 mM EGTA. *J. Gen. Physiol.* 106:259–336.

Pape, P. C., D. S. Jong, and W. K. Chandler. 1998. Effects of partial sarcoplasmic reticulum calcium depletion on calcium release in frog cut muscle fibers equilibrated with 20 mM EGTA. *J. Gen. Physiol.* 112:263–295.

Pape, P. C., D. S. Jong, W. K. Chandler, and S. M. Baylor. 1993. Effect of fura-2 on action potential-stimulated calcium release in cut twitch fibers from frog muscle. *J. Gen. Physiol.* 102:295–332.

Pizarro, G., N. Shirokova, A. Tsugorka, and E. Ríos. 1997. "Quantal" calcium release operated by membrane voltage in frog skeletal muscle. *J. Physiol.* 509:289–303.

Richard, E. A., and C. Miller. 1990. Steady-state coupling of ion-channel conformations to a transmembrane ion gradient. *Science*. 247: 1208–1210.

Ríos, E., and G. Pizarro. 1991. Voltage sensor of excitation-contraction coupling in skeletal muscle. *Physiol. Rev.* 71:849–908.

Rome, L. C., D. A. Syme, S. Hollingworth, S. L. Lindstedt, and S. M. Baylor. 1996. The whistle and the rattle: the design of sound producing muscles. *Proc. Natl. Acad. Sci. U.S.A.* 93:8095–8100.

Schneggenburger, R., and P. Ascher. 1997. Coupling of permeation and gating in an NMDA-channel pore mutant. *Neuron.* 18:167–177.

Schneider, M. F., E. Ríos, and W. Melzer. 1987a. Determining the rate of calcium release from the sarcoplasmic reticulum in muscle fibers. *Biophys. J.* 51:1005–1007.

Schneider, M. F., and B. J. Simon. 1988. Inactivation of calcium release from the sarcoplasmic reticulum in frog skeletal muscle. *J. Physiol.* 405:727–745.

Schneider, M. F., B. J. Simon, and G. Szucs. 1987b. Depletion of calcium from the sarcoplasmic reticulum during calcium release in frog skeletal muscle. *J. Physiol.* 392:167–192.

Schuster, S., M. Marhl, and T. Höfer. 2002. Modeling of simple and complex calcium oscillations. From single-cell responses to intercellular signaling. *Eur. J. Biochem.* 269:1333–1355.

Sham, J. S., L. S. Song, Y. Chen, L. H. Deng, M. D. Stern, E. D. Lakatta, and H. Cheng. 1998. Termination of Ca^{2+} release by a local inactivation of ryanodine receptors in cardiac myocytes. *Proc. Natl. Acad. Sci. U.S.A.* 95:15096–15101.

Shirokova, N., J. Garcia, G. Pizarro, and E. Rios. 1996. Ca^{2+} release from the sarcoplasmic reticulum compared in amphibian and mammalian skeletal muscle. *J. Gen. Physiol.* 107:1–18.

Shirokova, N., G. Pizarro, and E. Ríos. 1994. A damped oscillation in the intramembranous charge movement and calcium release flux of frog skeletal muscle fibers. *J. Gen. Physiol.* 104:449–476.

Smith, G. D., L. Dai, R. M. Miura, and A. Sherman. 2001. Asymptotic analysis of buffered calcium diffusion near a point source. *SIAM J. Appl. Math.* 61:1816–1838.

Stern, M. D. 1992. Buffering of calcium in the vicinity of a channel pore. *Cell Calcium.* 13:183–192.

Stern, M. D., G. Pizarro, and E. Rios. 1997. A local control model of excitation-contraction coupling in skeletal muscle. *J. Gen. Physiol.* 110:415–440.

Stern, M. D., L. S. Song, H. Cheng, J. S. Sham, H. T. Yang, K. R. Boheler, and E. Ríos. 1999. Local control models of cardiac excitation-contraction coupling: a possible role for allosteric interactions between ryanodine receptors. *J. Gen. Physiol.* 113:469–489.

Wang, S. -Q., L.-S. Song, L. Xu, G. Meissner, E. G. Lakatta, E. Ríos, M. D. Stern, and H. Cheng. 2002. Thermodynamically irreversible gating of ryanodine receptors in situ revealed by stereotyped duration of release in Ca^{2+} sparks. *Biophys. J.* 83:242–251.

Yu, S. P., L. M. Canzoniero, and D. W. Choi. 2001. Ion homeostasis and apoptosis. *Curr. Opin. Cell Biol.* 13:405–411.